Survey and Analysis of Cyclostationary Signal Detector Implementations on FPGA

Marko Kosunen, *Member, IEEE*, Vesa Turunen, *Student Member, IEEE*, Kari Kokkinen, *Student Member, IEEE*, and Jussi Ryynänen, *Member, IEEE*

***Abstract*—Detecting the presence of primary users and ability to find white spaces in the spectrum are the key enablers of the opportunistic communication. This paper analyzes the trade-offs in cyclostationary-based spectrum sensing algorithm implementations in terms of performance, hardware complexity, and power consumption. The evaluation of the algorithm implementations is performed on field-programmable gate arrays. The analysis presented will provide the designer understanding of dependency between algorithm complexity and power consumption, which is inherently limiting factor of implementation feasibility for cognitive mobile devices.**

***Index Terms*—Cognitive radio, detection algorithms, field-programmable gate array (FPGA), spectrum sensing.**

I. Introduction

THE RIGID allocation and control of spectrum resources, i.e., the current practice of licensing the frequency space to primary users, has led to a situation in which emerging new wireless technologies lack spectrum resources for communication. A licensed frequency band is reserved for the primary user even though it is not currently occupied by active signal transmission. Cognitive radios have been proposed to alleviate this problem by sensing the availability of free spectral resources and utilizing the detected resource for communication in an opportunistic manner [1], [2]. The key enabler of cognitive radio is the spectrum sensor, which is responsible for the detection of the primary user (PU) on a licensed band. The sensitivity of the sensor should exceed the sensitivity of the receiver belonging to the primary system. This is mandatory in order to prevent the interference from the secondary communication on the licensed band.

Several sensing algorithms have been proposed and analyzed recently [3]–[6]. Most of them utilize an energy detector for sensing of the presence of the primary user [4]. This is due to the observation that so far cyclostationary detectors have relatively high computational complexity and complex implementations [2].

On the other hand, energy detectors, although ideal for spectrum sensing in theory, are not, in all cases, suitable for practical application which requires signal detection in a negative signal-to-noise-ratio (SNR) regime. This is due to their susceptibility to uncertainties in the receiver noise level [7].

In this paper, implementations of various detection algorithms based on autocorrelation and cyclostationary features are presented and analyzed. The aim is to compare suitable implementations for mobile spectrum sensing devices, and give examples of the level of computational complexity of the algorithms that are implementable on mobile devices in terms of power consumption. The performance, implementation complexity and power consumption of several implementations are analyzed on the same field-programmable gate array (FPGA) implementation platform in order to produce comparable results and determine unambiguously the effect of design choices to the quality of implementation. To our knowledge, this is the first paper presenting comprehensive analysis and comparable results for effect of design choices in hardware implementations of various spectrum sensing algorithms. It is demonstrated that by avoiding resource consuming operations such as fast Fourier transform (FFT) and matrix inversion, and by using algorithms, such as CORDIC, that are well suited for hardware implementations, it is possible to achieve a reduction of an order of magnitude in power dissipation without compromising the performance.

An extensive implementation comparison of various spectrum sensing algorithms extends the previously published analysis on the implementation complexities of angular computation-based algorithms [8] to cover the implementations of recent autocorrelation- and cyclostationary-based detection algorithms suitable for a mobile low-power operating environment. Furthermore, alternative computation methods for angular domain test statistics are described and analyzed, and performance and implementation complexities are compared to energy detector implementation, which can be considered as the simplest reference.

In this paper, it is shown that by reformulating the known algorithms to use only computation that is well suited to implementation on-silicon will result in a tenfold reduction of power dissipation and while preserving efficient low-SNR detection. The effects of implementation-performance trade-offs are addressed in order to demonstrate the benefits in implementation gained by accepting minor performance degradation from theoretically optimal performance.

Manuscript received April 29, 2013; revised July 03, 2013; accepted July 23, 2013. Date of publication October 01, 2013; date of current version December 09, 2013. This work was supported in part by the European Union, in part by the Finnish Funding Agency for Technology and Innovation, and in part by Nokia Research Center. This paper was recommended by Guest Editor R. Gomez-Garcia.

M. Kosunen and J. Ryynänen are with the Department of Micro and Nanosciences, School of Electrical Engineering, Aalto University, 00076 Espoo, Finland (e-mail: marko.kosunen@aalto.fi; jussi.ryynanen@aalto.fi).

V. Turunen and K. Kokkinen are with Renesas Mobile, 00180 Helsinki, Finland (e-mail: vesa.turunen@aalto.fi; kari.kokkinen@iki.fi).

Digital Object Identifier 10.1109/JETCAS.2013.2280810

The detection performance of the algorithms is evaluated in an additive white Gaussian noise (AWGN) channel with an orthogonal frequency-division multiplexed (OFDM) signal that has a similar symbol structure to that used in the digital video broadcasting—terrestrial (DVB-T) system. The AWGN channel is selected in order to provide first order estimate of their relative performance and performance trade-offs caused by simplifications in hardware implementation. More advanced analysis for example in fading channels is beyond the scope of this paper.

This paper is organized as follows. In Section II, the Neyman–Pearson hypothesis testing applied in all of the signal detection algorithms is presented. In Sections III–VIII, the actual algorithms and their implementations are described. In Section IX, the performance of the algorithms in the detection of an OFDM modulated signal is compared. The complexities of physical implementations are compared in Section X. Conclusions are drawn in Section XI.

II. Neyman–Pearson Hypothesis Test for Signal Detection

The algorithms analyzed in this paper apply the Neyman–Pearson criterion for hypothesis testing of the presence of the signal

$$\begin{aligned} \mathrm{H}_0: &\quad \hat{T} = \epsilon \\ \mathrm{H}_1: &\quad \hat{T} = T + \epsilon \end{aligned}$$

where $\hat{T}$ is the estimate of the detection test statistics produced as a result of the algorithm under consideration, ϵ is the contribution of noise to the test statistics and, T is the corresponding test statistic for the actual signal. The requirement for successful testing is that the presence of a signal causes an observable change to the value of the test statistics, and that the test statistics is a monotonic function of SNR.

For all the algorithms considered in this paper, the probability distribution and the cumulative distribution function $P(\hat{T} \leq \eta)$ of the test statistics under the hypothesis H_0 are known (no signal, only noise present). Therefore the decision threshold for the $\hat{T}$ can be calculated as $\eta = P^{-1}(1 - P_{\mathrm{FA}})$, providing a constant false-alarm rate P_{FA} for detection.

In decision making, the null hypothesis H_0 is rejected when $\hat{T} \geq \eta$, and H_1 is assumed. Knowledge of distribution under H_1 is not required for testing, even though it can be determined at least for some of the algorithms. This results in a lack of well-defined *a priori* knowledge of the probability of detection P_D under H_1; however, the probability of detection as a function of the SNR can be evaluated by simulations. The performance of the algorithms can be compared by evaluating the detection sensitivity as a function of SNR. The comparison for the algorithms considered in this paper is presented in Section X.

A. Signal Definitions

In the context of this paper, the white Gaussian noise signal $x_n(n)$ is defined as a zero mean complex signal with Gaussian distributed uncorrelated real and imaginary parts each having the variance σ^2, thus resulting in the total variance of the complex Gaussian noise signal $2\sigma^2$.

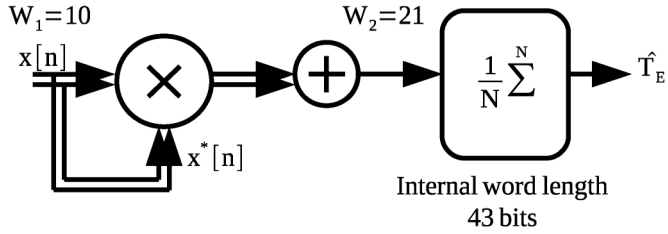

Fig. 1. Block diagram of a energy detector.

Circuitry for removing the dc component (the mean of the input signal), is implemented and is common to all of the hardware implementations presented in this paper. Being simple to implement, it has been left out from the figures in order to keep the presentation clear. Since the mean can be removed from the input signal with reasonable accuracy, the assumption of the zero mean can be considered valid.

III. Energy Detector

The test statistic used for the energy detector is the power of the input signal, which can be estimated as

$$\hat{T}_E = \frac{1}{N} \sum_{n=0}^{N-1} |x(n)|^2 . \tag{1}$$

For zero mean Gaussian noise, $(N/2\sigma^2)\hat{T}_E$ is a sum of squares of $2N$ standard normal random variables and is therefore χ^2-distributed with $2N$ degrees of freedom.

Let the probability of a false alarm in hypothesis testing be

$$P_{\mathrm{FA}} = 1 - P_{\chi^2_{2N}} \left(\frac{N}{2\sigma^2} \eta \right). \tag{2}$$

The decision threshold for the energy detector can then be computed as

$$\eta = \frac{2\sigma^2}{N} P^{-1}_{\chi^2_{2N}} (1 - P_{\mathrm{FA}}). \tag{3}$$

For the hypothesis test, the value of σ^2 is assumed to be known. This is the major weakness of this method since the variance of noise is dependent on several parameters such as the noise figure of the RF-front-end, which varies as a function of the operating modes of the receiver. In general, it is difficult to estimate the noise variance reliably [7], and therefore the usage of the energy detector would require noise calibration [9].

A. Implementation

The algorithm implementation block diagram of a energy detector is presented in Fig. 1.[1] It consists of two multipliers and a digital integrator. The result $\hat{T}_E$ is obtained for decision once in N clock cycles, thus defining the decision rate.

The energy detector is the simplest of the detection algorithm implementations and gives a good reference for the complexity of other implementations. Its power consumption is determined with an 85% contribution by the multipliers for computing the square of the absolute value of the input signal.

[1]In this paper, the double line presents real and imaginary parts of a complex-valued signal, and the triple line three parallel signal buses. Subscripted parameter W_x denotes the bus width of the nearest bus. Additional notes are used to provide information about the most relevant implementation parameters.

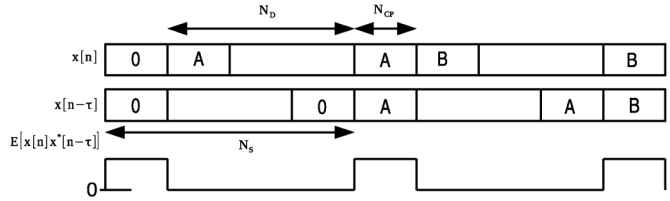

Fig. 2. General OFDM symbol structure with data, and cyclic prefixes. Correlating parts of the symbol are marked with 0, A, and B.

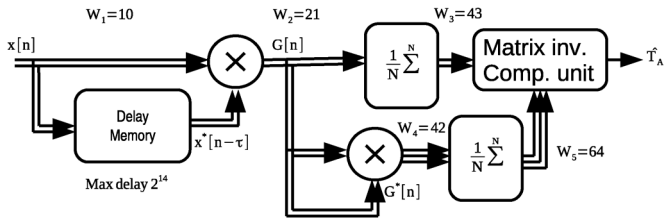

Fig. 3. Block diagram of a autocorrelation detector.

IV. Autocorrelation Feature Detector

Fig. 2 depicts a typical structure of an OFDM symbol. The OFDM symbol with a length N_S consists of actual the data contents with a length N_D a cyclic prefix with a length N_{CP}. The cyclic prefix is a copy of N_{CP} samples from the end of the symbol, added to the front of the symbol in order to reduce inter-symbol-interference and improve the system performance in a multipath propagation environment. The cyclic prefix can also be used for timing and frequency acquisition [10].

It can be observed from Fig. 2 that if the delay value used in autocorrelation is $\tau = N_D$, the product of the cyclic prefix and its corresponding complex conjugate at the end of the OFDM symbol will result in a magnitude-squared type of result. This generates positive-mean "pulses" with a period of N_S and a duration of N_{CP} samples. Outside the correlating part the expectation of $x(n)x^*(n-\tau)$ remains zero, as depicted in Fig. 2.

If the received signal is random Gaussian white noise, i.e., the real and imaginary parts are Gaussian random and uncorrelated, the expectation of the autocorrelation remains zero. This is the condition under the null hypothesis of the Neyman–Pearson test [11].

The test statistic for the autocorrelation detector can be computed as follows. The estimate of autocorrelation is first computed as

$$\hat{R}_a(\tau) = \frac{1}{N}\sum_{n=0}^{N-1} x(n)x^*(n-\tau) \tag{4}$$

$$= \frac{1}{N}\sum_{n=0}^{N-1} x_a(n) + jy_a(n) = X_a + jY_a. \tag{5}$$

To obtain test statistics, the real and imaginary parts of the autocorrelation estimate are arranged as a vector

$$\hat{r}_a = \left[\Re\left\{\hat{R}_a(\tau)\right\}\ \Im\left\{\hat{R}_a(\tau)\right\}\right] = [X_a\ Y_a]. \tag{6}$$

The test statistic is then computed as

$$\hat{T}_A = N\hat{r}_a\hat{\Sigma}_a^{-1}\hat{r}_a^T \tag{7}$$

where $\hat{\Sigma}_a$ is

$$\hat{\Sigma_a} = \begin{bmatrix} \hat{E}\left[X_a^2\right] & \hat{E}[X_aY_a] \\ \hat{E}[X_aY_a] & \hat{E}\left[Y_a^2\right] \end{bmatrix} \tag{8}$$

$$= \begin{bmatrix} A & B \\ C & D \end{bmatrix}. \tag{9}$$

The method is similar to that presented in [12], but without frequency shift by the cyclic frequency α.

Under the null hypothesis, the test statistic is χ_2^2 distributed, and therefore the decision threshold is obtained from the inverse of the cumulative distribution function of the χ_2^2-distribution

$$\eta_A = F_{\chi_2^2}^{-1}(1 - P_{\mathrm{FA}}). \tag{10}$$

In order to give an insight into the hardware required for obtaining the test statistics, the computation is presented here in detail. Using notation from (5), the elements of $\hat{\Sigma}$ can be estimated as

$$\hat{E}\left[X_a^2\right] = \frac{1}{N}\sum_{n=0}^{N-1} x_a^2(n) = A \tag{11}$$

$$\hat{E}[X_aY_a] = \frac{1}{N}\sum_{n=0}^{N-1} x_a(n)y_a(n) = B = C \tag{12}$$

$$\hat{E}\left[Y_a^2\right] = \frac{1}{N}\sum_{n=0}^{N-1} y_a^2(n) = D. \tag{13}$$

The inversion of a 2×2 matrix is relatively simple to compute, and therefore suitable for hardware implementation

$$\hat{\Sigma}^{-1} = \frac{1}{AD - BC}\begin{bmatrix} D & -B \\ -C & A \end{bmatrix}. \tag{14}$$

Taking into account that in (14) $B = C$, the test statistics can be computed as

$$T_A = \frac{X_a^2\hat{E}\left[Y_a^2(n)\right] + Y_a^2\hat{E}\left[X_a^2(n)\right] - 2X_aY_a\hat{E}\left[X_a(n)Y_a(n)\right]}{\hat{E}\left[X_a^2(n)\right]\hat{E}\left[Y_a^2(n)\right] - \left(\hat{E}\left[X_a(n)Y_a(n)\right]\right)^2}. \tag{15}$$

A. Implementation

Fig. 3 depicts the implementation of the autocorrelation detector. A memory element for the real and imaginary parts of the signal is required to implement the autocorrelation delay, which is determined by τ. Whereas the energy detector used two multipliers for computing the square of the absolute value of the input signal, in the autocorrelation detector a full complex multiplier is required to compute the autocorrelation. Additionally, a matrix inverse computation unit is required. It consists of five multipliers, three adders and a division computation unit.

The sampling rate for the matrix inversion computation unit is F_s/N, N being the number of samples required for reliable detection. With a sufficiently large N, multiple clock cycles can be used to compute the division used in the inversion with an iterative algorithm.

In the autocorrelation detector, the added complexity and increased power consumption compared to the energy detector are

due to the delay memory and complex multiplier for autocorrelation computation (45% of power consumption) and the multipliers and division computation units for matrix inversion and the computation of the test statistics (45%).

A simplified implementation of an autocorrelator detector using only the real part of the autocorrelation is presented in [13]. Although the implementation is very simple, it suffers from sensitivity to frequency offset, which is avoided by using both the real and imaginary parts of the autocorrelation in decision making.

V. Cyclostationary Feature Detector With Frequency Domain Test Statistics Computation

The algorithm and its implementation follow the idea originally presented in [12]. The signal is said to be cyclostationary if its time varying expectation of (auto)covariance, i.e., autocorrelation

$$E\left[x(n)x^*(n-\tau)\right] \tag{16}$$

is periodic, i.e., can be presented with some set of Fourier coefficients [12].

If the autocorrelation is periodic for some delay τ, as is the case for the OFDM signal as presented in Fig. 2, then its frequency component at some cyclic frequency α is nonzero. This component, cyclic autocorrelation, can be estimated as with N observations as [12]

$$\hat{R}(\tau,\alpha) = \frac{1}{N}\sum_{n=0}^{N-1} x(n)x^*(n-\tau)e^{-j\frac{2\pi\alpha n}{N}}. \tag{17}$$

The estimate is a single frequency component from the discrete-time Fourier transform of $x(n)x^*(n-\tau)$

$$F(k) = \frac{1}{N}\sum_{n=0}^{N-1} x(n)x^*(n-\tau)e^{-j\frac{2\pi k n}{N}} \tag{18}$$

$$= X(k) + jY(k) \tag{19}$$

at a frequency $k = \alpha$.

The statistical test for the existence of cyclostationarity can be performed with test statistics computed in the frequency domain as presented in [12] and [5]. First, the real and imaginary parts of the cyclic autocorrelation estimate are arranged as a vector

$$\hat{r} = \left[\Re\left\{\hat{R}(\tau,\alpha)\right\}\ \Im\left\{\hat{R}(\tau,\alpha)\right\}\right] \tag{20}$$

$$= \left[X(\alpha)\ Y(\alpha)\right]. \tag{21}$$

As for the autocorrelator detector, the test statistics for the hypothesis testing can then be computed with the method presented in [12]

$$\hat{T}_C = N\hat{r}\hat{\Sigma}^{-1}\hat{r}^T \tag{22}$$

where

$$\hat{\Sigma} = \begin{bmatrix} \hat{E}\left[X^2(k)\right] & \hat{E}\left[X(k)Y(k)\right] \\ \hat{E}\left[X(k)Y(k)\right] & \hat{E}\left[Y^2(k)\right] \end{bmatrix} \tag{23}$$

$$= \begin{bmatrix} A & B \\ C & D \end{bmatrix}. \tag{24}$$

Under the null hypothesis, the test statistic is χ_2^2 distributed [12], and therefore the decision threshold is obtained from

$$\eta_C = F^{-1}_{\chi_2^2}(1-P_{\mathrm{FA}}). \tag{25}$$

Compared to the autocorrelator, the $\hat{\Sigma}$ of the frequency domain cyclostationary detector is computed in the same way but from the frequency domain signal. The elements of $\hat{\Sigma}$ can be estimated as

$$\hat{E}\left[X^2(k)\right] = \frac{1}{N}\sum_{n=0}^{N-1} X^2(k) = A \tag{26}$$

$$\hat{E}\left[X(k)Y(k)\right] = \frac{1}{N}\sum_{n=0}^{N-1} X(k)Y(k) = B = C \tag{27}$$

$$\hat{E}\left[Y^2(k)\right] = \frac{1}{N}\sum_{n=0}^{N-1} Y^2(k) = D. \tag{28}$$

Finally, the test statistics can be written as (29) shown at bottom of the page.

A. Implementation

Fig. 4 depicts the implementation block diagram of the cyclostationary feature detector with frequency-domain test statistics computation. The programmable decimator is realized with a cascaded integrator-comb (CIC) [14] and canonic signed digit FIR filters [15] in order to achieve low power dissipation. The Radix-2^2 architecture is used for the FFT computation unit [16], [17]. The implementation of the detector is presented in detail in [18].

The advantage of the cyclostationary feature detector compared to the autocorrelation detector is its insensitivity to narrowband interferers. Narrowband interferers can be present for example, as a result of the clock signal feedthrough, and are often present in wireless receivers. These interferers provide strong complex autocorrelation components at zero frequency, regardless of their original frequency. If the OFDM symbol is long, the cyclic frequency α is very low. In this case the cyclic frequency component can be masked by the interference caused by the narrowband signals. Because the frequency resolution of the FFT is proportional to F_s/N, the problem can be alleviated by increasing N or reducing F_s. Increasing the length N of the FFT-unit would result in a remarkably high power consumption.

$$T_C = \frac{X^2(\alpha)\hat{E}\left[Y^2(k)\right] + Y^2(\alpha)\hat{E}\left[X^2(k)\right] - 2X(\alpha)Y(\alpha)\hat{E}\left[X(k)Y(k)\right]}{\hat{E}\left[X^2(k)\right]\hat{E}\left[Y^2(k)\right] - \left(\hat{E}\left[X(k)Y(k)\right]\right)^2} \tag{29}$$

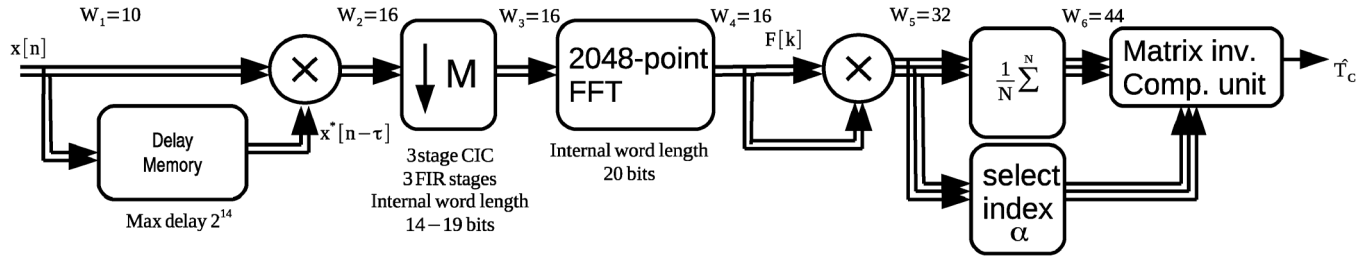

Fig. 4. Implementation block diagram of the frequency-domain cyclostationary feature detector.

Therefore the decimator is used to reduce the sampling rate and increase the resolution. Effectively, it multiplies the α relative to the sampling frequency. The maximum decimation factor M is $\lfloor F_s/\alpha \rfloor$. The filtering in decimation increases the effective signal to noise ratio by M because with α being low, only the noise is filtered, while the power of the cyclic frequency component remains.

The power dissipation of the cyclostationary feature detector utilizing frequency domain test statistic computation is contributed mainly by the FFT (42%) decimator (26%), and the autocorrelator (20%).

Increasing the decimation ratio reduces the power consumption of the FFT, but increases the power consumption of the decimator. The overall energy consumption of the FFT is constant, because the decimation increases the time used for FFT computation, respectively, also increasing the time used for detection.

VI. Time-Domain Cyclostationary Feature Detector

Although the cyclostationary detector with frequency-domain test statistic is feasible to implement, and could provide a means for observation of multiple cyclic frequencies simultaneously, it can be observed that fundamentally there is no need to calculate the FFT, which makes a major contribution to power dissipation.

The feature of interest is the relative strength of a cyclic frequency component of the autocorrelation to the average variance of the autocorrelation signal. However, all the information required to compute this is already available in the time domain.

For a single cycle frequency, the cyclic autocorrelation function in (17) is a frequency shifted autocorrelation of the input signal. Frequency shift can be efficiently performed with the CORDIC algorithm, which has been used for the computation of trigonometric functions, their inverses, and for the modulation of signals in digital transmitters [19]–[22].

The test statics

$$\hat{T}_T = N\hat{r}\hat{\Sigma}^{-1}\hat{r}^T \tag{30}$$

can also be computed directly from the real and imaginary parts of (17) without the FFT

$$\hat{r} = \left[\Re\left\{\hat{R}(\tau,\alpha)\right\}\ \Im\left\{\hat{R}(\tau,\alpha)\right\}\right] \tag{31}$$

$$= \left[X_t(\alpha)\ Y_t(\alpha)\right]. \tag{32}$$

The components of the correlation matrix are also computed in the time domain, resulting in an otherwise identical result with the autocorrelator detector.

By denoting

$$x(n)x^*(n-\tau)e^{-j\frac{2\pi\alpha n}{N}} = x_t(n,\alpha) + jy_t(n,\alpha) \tag{33}$$

the elements of the covariance matrix can be computed as

$$\hat{E}\left[X_t^2(\alpha)\right] = \frac{1}{N}\sum_{n=0}^{N-1} x_t^2(n,\alpha) = A \tag{34}$$

$$\hat{E}\left[X_t(\alpha)Y_t(\alpha)\right] = \frac{1}{N}\sum_{n=0}^{N-1} x_t(n,\alpha)y_t(n,\alpha)$$

$$= B = C \tag{35}$$

$$\hat{E}\left[Y_t^2(\alpha)\right] = \frac{1}{N}\sum_{n=0}^{N-1} y_t^2(n,\alpha) = D. \tag{36}$$

Applying the matrix inversion, the final test statistic is computed as in (37) shown at the bottom of the page.

A. Implementation

Fig. 5 depicts the implementation block diagram of the time-domain cyclostationary feature detector. The decimator and FFT computation block of the frequency-domain cyclostationary detector are replaced by the CORDIC computation block. The selector circuit for the frequency component is replaced by an integrator and complex multiplier, providing the necessary values $X^2(\alpha)$, $Y^2(\alpha)$, and $X(\alpha)Y(\alpha)$ to the matrix inversion unit.

By time-domain computation, the decimator and FFT computation block of the frequency-domain cyclostationary

$$T_T = \frac{X_t(\alpha)^2\hat{E}\left[Y_t(\alpha)^2\right] + Y_t(\alpha)^2\hat{E}\left[X_t(\alpha)^2\right] - 2X_t(\alpha)Y_t(\alpha)\hat{E}\left[X_t(\alpha)Y_t(\alpha)\right]}{\hat{E}\left[X_t(\alpha)^2\right]\hat{E}\left[Y_t(\alpha)^2\right] - \left(\hat{E}\left[X_t(\alpha)Y_t(\alpha)\right]\right)^2} \tag{37}$$

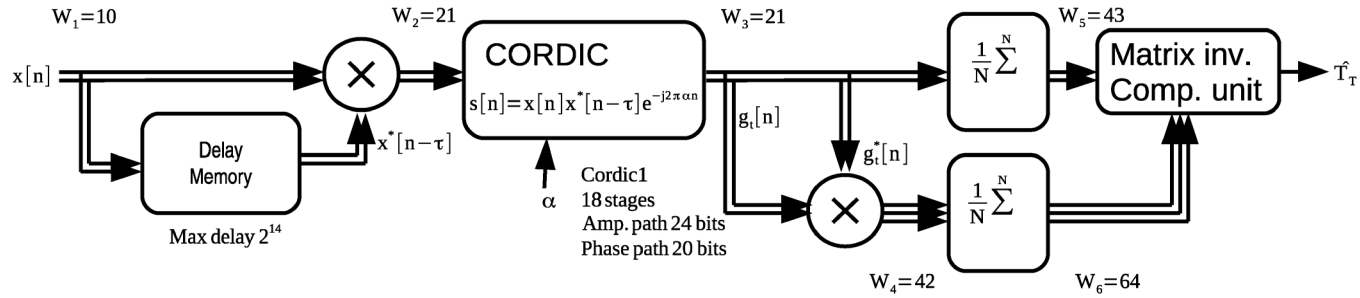

Fig. 5. Time-domain cyclostationary detector.

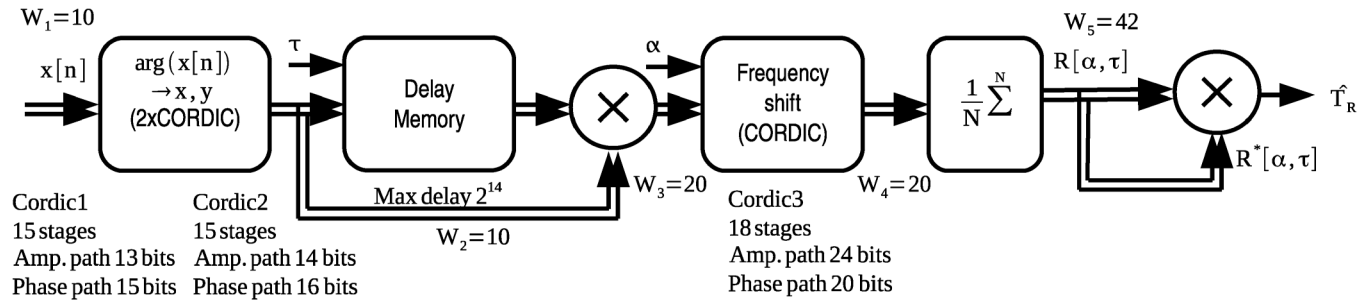

Fig. 6. Spatial sign cyclic correlation detector.

detector are eliminated without compromising the performance, resulting in significant hardware reductions. The power consumption is mainly contributed by the autocorrelation computation (34%), CORDIC for the frequency shift (11%), and the multipliers and division units for matrix inversion computation (45%).

In the CORDIC frequency shifter, the frequency resolution is set by appropriate word lengths and the number of stages, providing more flexible structure in contrast to the frequency domain implementation where in order to double the frequency resolution, twice as large an FFT has to be implemented.

VII. Spatial Sign Cyclic Correlation Detector

The spatial sign cyclic correlation detector [23] is based on the observation that the cyclic frequency components are also present in the autocorrelation of the spatial sign function of the complex input data. The spatial sign function of the input signal $x(n)$ is calculated as

$$s(n) = \begin{cases} \frac{x(n)}{|x(n)|}, & x(n) \neq 0 \\ 0, & x(n) = 0 \end{cases}. \tag{38}$$

The spatial sign cyclic correlation estimator can be calculated as presented in [23]

$$\hat{R}(\tau, \alpha) = \frac{1}{N} \sum_{n=0}^{N-1} s(n) s^*(n-\tau) e^{-j\frac{2\pi\alpha n}{N}}. \tag{39}$$

For the testing of the hypotheses, the test statistic can be calculated from the spatial sign cyclic correlation estimator as

$$\hat{T}_R = 2N \left(\Re\left\{ \hat{R}(\tau, \alpha) \right\}^2 + \Im\left\{ \hat{R}(\tau, \alpha) \right\}^2 \right). \tag{40}$$

Because of the normalization, the covariance matrix is replaced by a constant, resulting in simplified computation of the test statistic.

The test statistic $\hat{T}_R$ is χ_2^2 distributed, resulting in the decision threshold

$$\eta_R = F_{\chi_2^2}^{-1}(1 - P_{\mathrm{FA}}). \tag{41}$$

It should be observed, that as a result relationship of χ^2 and γ distribution $T_r/2$ is γ-distributed with the shape factor $k = 1$ [23].

A. Implementation

Fig. 6 depicts the implementation block diagram of the spatial sign cyclic correlator detector.

From the implementation point of view the main benefit gained when compared to the time domain cyclostationary feature detector is the simplified computation of the test statistics as a result of the normalization of the signal amplitude, resulting in a reduced amount of hardware and significantly reduced power dissipation. The cost of simplification in computation of the test statistic is the two additional CORDICs required for the computation of the spatial sign function; however, their power consumption is small compared to the CORDIC for the frequency shift. The overall contribution of CORDICs is 24%. The main contributor to the power consumption is the autocorrelation computation unit (62%) consisting of the complex multiplier and the delay memory.

VIII. Spatial Sign Cyclic Correlator With Angular Domain Computation

In angular domain spatial sign cyclic correlators [8], the spatial sign function is rewritten using exponential presentation of complex numbers as

$$s(n) = \begin{cases} e^{j\phi_x(n)}, & x(n) \neq 0 \\ 0, & x(n) = 0 \end{cases} \tag{42}$$

$$\phi_x(n) = \angle x(n). \tag{43}$$

Using the notation of (42), the spatial sign cyclic correlation estimator (39) can be written as

$$\hat{R}(\tau,\alpha) = \frac{1}{N}\sum_{n=0}^{N-1} e^{j\phi_x(n)} e^{-j\phi_x(n-\tau)} e^{-j\frac{2\pi\alpha n}{N}} \tag{44}$$

$$= \frac{1}{N}\sum_{n=0}^{N-1} e^{j\phi_x(n)-j\phi_x(n-\tau)-j\frac{2\pi\alpha n}{N}} \tag{45}$$

$$= \frac{1}{N}\sum_{n=0}^{N-1} e^{j\phi_T(n)} \tag{46}$$

$$\phi_T(n) = \phi_x(n) - \phi_x(n-\tau) - \frac{2\pi\alpha n}{N}. \tag{47}$$

Under the null hypothesis H_0 of the Neyman–Pearson test the input signal contains only Gaussian white noise. For Gaussian noise $\phi_T(n)$ in uniformly distributed $\phi_T(n) \sim U(0, 2\pi)$. Under H_1 the distribution of $\phi_T(n)$ is dependent on the ratio N_{CP}/N_F and SNR. However, the knowledge of the actual distribution under H_1 is not required for successful hypothesis testing.

In order to avoid the implementation of hardware for angular-to-Cartesian conversion as in the spatial sign cyclic correlator, it is preferable to perform the hypothesis test in the angular domain by testing the uniformity of the angle distribution. To test the uniform distribution, the angle $\phi_T(n) \in [0 \ldots 2\pi]$ is categorized in M even-sized bins, resulting in a set of i.i.d. binomially distributed random variables

$$Z_k\left(\phi_T(n)\right) \sim B\left(N, \frac{1}{M}\right), \quad k \in [0, M-1] \tag{48}$$

where N is the total number of samples used for the current test. With $Z_k(\phi_T(n))$ a test for uniform distribution can be performed.

For successful testing, M is constrained to $M > 2$, because $M = 2$ would provide false information about the distribution if $\phi_T(n)$ is distributed evenly across the bin border, although not uniformly over $[0 \ldots 2\pi)$. Because the phase value $\phi_T(n)$ is presented with fixed point 2's complement binary number, $M = 3$ would require additional hardware (subtraction units) for binning, compared to $M = 4$, in which the bin borders are determined by the two most significant bits of the $\phi(n)$. Therefore, from the implementation point of view, $M = 4$ is optimal.

A. Angular Domain Tests

1) Binomial Distribution Test: Since elements of $Z_k \sim B(N, 1/M)$, we may define the test statistic as

$$\hat{T}_{z,k} = Z_k \tag{49}$$

and the decision thresholds from the inverse cumulative binomial distribution $P = P_B^{-1}(z, 1/M)$ as

$$\eta_{BL} = P_B^{-1}\left(\frac{1-(1-P_{\mathrm{FA}})^{\frac{1}{M}}}{2}, \frac{1}{M}\right) \tag{50}$$

$$\eta_{BH} = P_B^{-1}\left(\frac{1+(1-P_{\mathrm{FA}})^{\frac{1}{M}}}{2}, \frac{1}{M}\right). \tag{51}$$

If $\hat{T}_{z,k} = Z_k$ exceeds these thresholds for any k, then it is assumed that $\phi(n)$ is not uniformly distributed, and the null hypothesis H_0 is rejected.

2) Gaussian Distribution Test: With a sufficiently large N, the elements of Z_k are approximately $N(\mu_z, \sigma_z)$-distributed where

$$\mu_z = \frac{N}{M} \tag{52}$$

$$\sigma_z = \sqrt{\frac{N}{M}\left(1-\frac{1}{M}\right)}. \tag{53}$$

It is now possible to define two decision thresholds as in the previous case as

$$\eta_{NL} = P_{N(0,1)}^{-1}\left(\frac{1-(1-P_{\mathrm{FA}})^{\frac{1}{M}}}{2}\right)\sigma_z + \mu_z \tag{54}$$

$$\eta_{NH} = P_{N(0,1)}^{-1}\left(\frac{1+(1-P_{\mathrm{FA}})^{\frac{1}{M}}}{2}\right)\sigma_z + \mu_z \tag{55}$$

where $P_{N(0,1)}^{-1}$ is the inverse of cumulative standard normal distribution.

Basically the difference between binomial and Gaussian tests is only in decision the threshold, which should converge to the same values as the number of samples N increases. The implementations are otherwise identical.

3) χ^2-Test: With Gaussian distribution approximation, the χ^2 test can also be applied. Let

$$T_{\chi N} = \sum_{k=0}^{M-1}\left(\frac{(Z_k-\mu_z)}{\sigma_z}\right)^2. \tag{56}$$

$T_{\chi N}$ is approximately χ^2_{M-1} distributed, the decision threshold for the χ^2 test can be calculated as

$$\eta_{\chi N} = P_{\chi^2_{M-1}}^{-1}(1-P_{\mathrm{FA}}). \tag{57}$$

If the test statistic $T_{\chi N}$ exceed the threshold, $\phi_T(n)$ is assumed to be nonuniform, and H_0 is discarded.

B. Implementation

Fig. 7 depicts the implementation block diagram of the spatial sign cyclic correlator with angular domain computation.

The most remarkable improvements in implementation efficiency, when compared to the regular spatial sign cyclic correlator, are due to the following reductions in the hardware.

- Moving from the Cartesian to the angular domain reduces the number of signal paths from two (real and imaginary part) to one (phase). Because of this, the amount of memory can be halved.

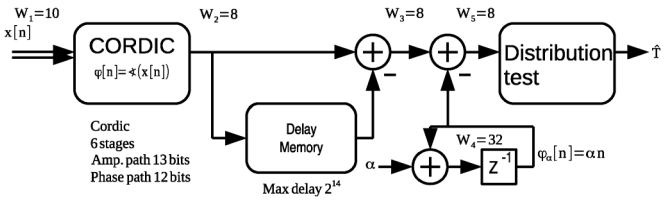

Fig. 7. Spatial sign cyclic correlator with angular domain computation.

- Complex multipliers are no longer required for the computation of autocorrelation. The complex multiplier is replaced by a single adder.
- Because the phase value is 2π periodic, there is no need to avoid overflows in phase domain computation. This results in reduced number of bits in computation.

The structure required for the classification of the $\phi_T(n)$ to M bins is identical in the binomial, Gaussian, and χ^2 tests. The χ^2 test requires a squaring unit and summation unit in addition.

Regardless of the computation method used for the test statistic, the savings in area and power are achieved as a result fact that angular domain computation requires only one signal branch instead of two for the complex I/Q-signal. Computation of the autocorrelation as a sum of the phases in the angular domain also eliminates the complex multiplier required for autocorrelation. Performing the testing directly from the angular domain signal also eliminates the CORDIC unit required for polar-to-Cartesian conversion. It can be stated that the angular domain computation eliminates all of the main contributors to the power dissipation of the spatial sign cyclic correlator but the delay memory, which clearly dominates the power consumption of this implementation with a contribution of 81%.

IX. Performance Comparison

Following abbreviations are used energy detector (EDET), autocorrelation detector (ACORR), cyclostationary feature detector with frequency domain test statistics computation (CYCFREQ), time-domain cyclostationary feature detector (CYCTIM), spatial sign cyclic correlation detector (SSCC), and spatial sign cyclic correlator with angular domain computation (ADSSCC).

The signal detection performances of the algorithms as a function of SNR are presented in Fig. 8, and the receiver operating characteristics are presented in Fig. 9. The signal used for evaluation is an OFDM signal with a similar symbol structure to that which is used in DVB-T, i.e., $N_{SYM} = 8192$ samples and $N_{CP} = 1024$ samples. The sampling rate corresponding to the DVB-T system sampling rate is 9.1429 Ms/s. $N = 524288$ samples per detection are used for detection in all simulation cases, resulting in a constant detection time $T_{det} = 57.4$ ms. The performances of the various angular domain distribution tests described in Section VIII-A are presented in Fig. 10. It can be observed from the detection probability curves of Fig. 8 and ROC-curves of Fig. 9 that the energy detector provides the best sensitivity, but the simulation does not take into account its sensitivity to the uncertainty in the noise variance estimate [7]. Therefore, the energy detector should be considered as an ideal reference design in terms of performance and implementation complexity. Reliable energy detection would require a reliable

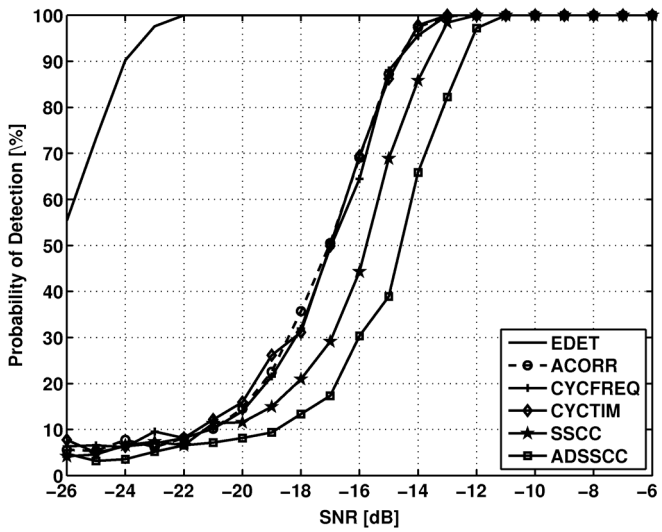

Fig. 8. Performance of the various detector implementations as a function of SNR, $P_{\mathrm{FA}} = 0.05$. The ADSSCC utilizes the binomial distribution test statistic computation. Because the inaccuracy of noise variance estimate is not taken into consideration, energy detector can be considered as ideal reference.

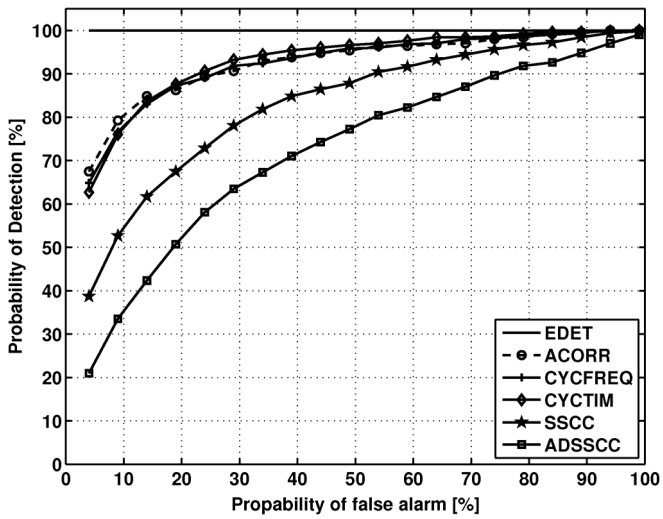

Fig. 9. Receiver operating characteristics of the detectors ($\mathrm{SNR} = -16$ dB).

noise calibration method to be implemented together with the detector, whereas the proposed cyclostationary algorithms does not require exact knowledge of the noise variance to perform reliably. Therefore, the main task is to find cyclostationary detectors with implementation complexity and power dissipation comparable with the energy detector.

The angular domain detectors are unquestionably least sensitive. However, the sensitivity of all the autocorrelation based algorithms with $P_{\mathrm{FA}} = 0.05$ lies within the range of 2 dB, which can be considered small from practical point of view. The reduced sensitivity can be compensated, for example, by using longer detection times as in Fig. 11, and thus reduced sensitivity is acceptable if the power consumption of the implementation is remarkably lower.

In Section X it is shown that by accepting 2 dB lower relative sensitivity of the sensing algorithm, the power consumption of the implementation can be reduced by the order of magnitude.

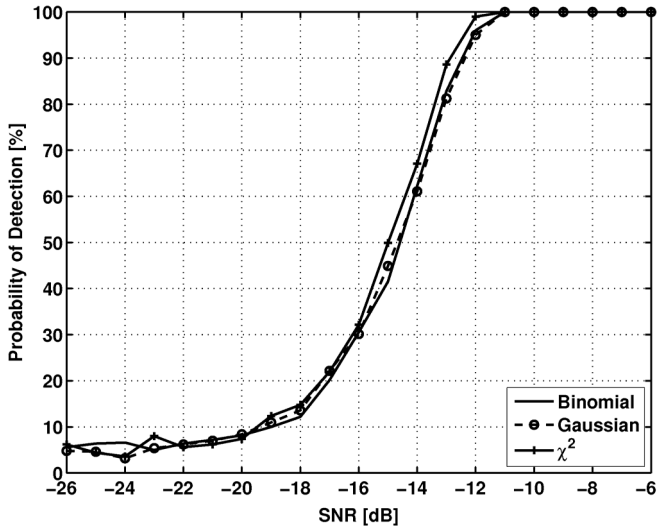

Fig. 10. Performance of the various angular domain distribution tests as a function of SNR.

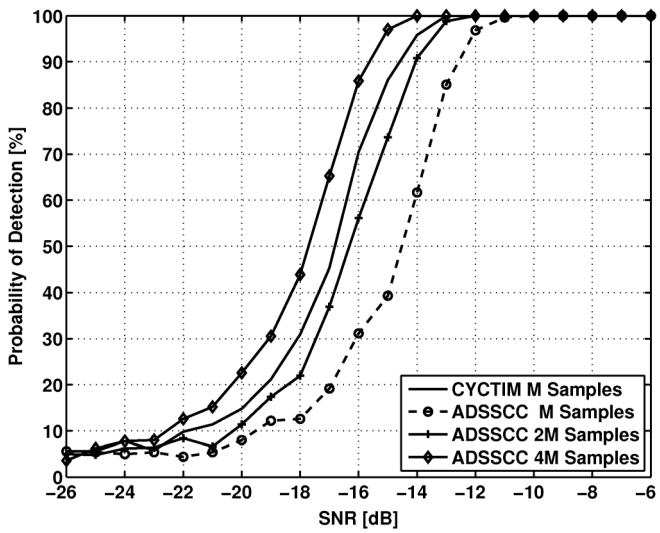

Fig. 11. Performance of the spatial sign cyclic correlator with angular domain test statistic using various sensing times, compared to Time domain cyclostationary detector.

However, the overall efficiency of the detection is strongly dependent on the implementation, settling time and power consumption of the RF front-end of the spectrum sensing receiver, and whether it is possible to efficiently use duty cycling during the sensing or not.

X. Implementation Comparison

In order to determine the differences in the computational complexity and power dissipation, the algorithms were described with RTL-level VHDL-description language and synthesized on 65 nm CMOS FPGA, which is a part of the algorithm implementation evaluation environment described in more detail in [24]. All the designs were compiled from RTL-level VHDL to FPGA-platform with the same compilation parameters. FPGA specific optimization parameters/structures were not used in order to maintain portability to other platforms.

TABLE I
Comparison of the Implementation Complexities

	Power [mW]	Logic	Registers	Memory [bits]	9b-multip.
EDET	2.69	612	290	0	0
ACORR	35.29	6779	1060	327680	234
CYCFREQ	61.29	16591	8802	405674	76
CYCTIM	34.99	8593	1291	327680	234
SSCC	20.90	5044	811	327680	32
ADSSCC	5.48	945	198	131072	0

TABLE II
Comparison of the Power Consumption

	EDET	ACORR	CYCFREQ	CYCTIM	SSCC	ADSSCC
FFT			25.44			
CORDICs				3.69	5.01	0.6
Decimator			16.02			
Autocorr.		15.77	12.37	11.88	12.96	4.45
Magn. comp.	2.28	1.71		1.47		
Tstats.	0.41	16.03	6.24	15.84	1.23	0.43
Other		1.78	1.22	2.11	1.7	
Total [mW]	2.69	35.29	61.29	34.99	20.9	5.48

The hardware complexity and power consumption of the algorithm implementations were evaluated with the the design tool of the FPGA vendor. The switching activity of the signals in the implementations was obtained with simulator and imported to the tool to improve the accuracy of the power consumption estimate. The complexity comparison is based on the numbers reported by the design tool, including the amount of logic elements (a four-input LUT), dedicated logic registers and on-chip memory (DPRAM). The design tool provides the hierarchical estimates of power consumption and reserved logic elements, registers, memory elements and multiplier units. The power consumption estimates reported are for total power consumption including both the static and dynamic power consumption, dynamic power consumption being clearly dominant.

All the implementations of the algorithms are evaluated using an 10-bit input word length and sampling rate of 20 Ms/s. The computation in the circuitry is performed with fixed point arithmetic. The word lengths used for number presentations and for internal computing inside the blocks are denoted in the corresponding implementation block diagrams to give further information on used hardware resources.

The implementation complexities and power dissipation estimates of various detector implementations are presented in Tables I and II, respectively. The angular domain spatial sign cyclic correlator uses the binomial distribution test for the test statistics computation.

The power consumption and implementation complexities can be summarized as follows. Cyclostationary feature detector with frequency domain test statistics computation (CYCFREQ) has the most complex implementation because of the FFT computation. Autocorrelation detector (ACORR) and cyclostationary feature detector with time domain test statistic computation (CYCTIM) consume less power because of lack

of FFT. They are almost equally complex because of the only difference is the CORDIC that is used for frequency shift and has relatively simple structure.

All of these three require quite a lot of hardware for test statistic computation, which results in large number of multipliers. The amount of hardware and power consumption could be reduced by further optimization of internal the word lengths. However, the computation still includes matrix inversion, which is quite resource consuming operation.

Implementation of spatial sign cyclic correlation detector (SSCC) consumes less hardware and power that the aforementioned detectors mainly because of the simpler computation of the test statistic. Because the signal, and thus test statistic is already normalized by CORDICs that have very simple implementation, the power consumption is dominated by delay and multiplications required for autocorrelation computation, which has 62% contribution of the overall power consumption.

The benefits of multiplierless implementation of Spatial sign cyclic correlator with angular domain computation (ADSSCC) are evident. The main reason for reduced power consumption is the fact that transformation from Cartesian to angular domain with CORDIC reduces the number of signal paths from two to one. In addition, the computation of autocorrelation can be performed with adders instead of multipliers which have negligible contribution to power consumption. The power consumption is almost entirely determined by the memory required for implementing the delay. The remarkably lower power dissipation of ADSSCC provides margin for compensation of the reduced sensitivity by increasing the number of samples (detection time) used per detection.

The power dissipation and area requirement for ASIC designs can be estimated by applying ratios between the FPGA and CMOS ASIC implementations, which are thoroughly analyzed in [25].

XI. Conclusion

In this paper, six implementations of signal detection algorithms for cognitive radio have been presented and analyzed in terms of performance, implementation complexity and power dissipation. The energy detector is used as the reference design indicating the lower limit of power dissipation that can be achieved. The comparison covers wide range of recently published autocorrelation and cyclostationary based detection algorithms suitable for a low-power operating environment. Also, alternative methods for the test statistic computation for Spatial sign cyclic correlator with angular domain computation have been analyzed.

The results indicate that the sensing algorithms containing complex computation such as FFT and matrix inversion, can be transformed to use computation well-suited for hardware implementations, such as CORDIC. With these modification, it is possible to achieve a reduction of an order of magnitude in power dissipation without compromising the performance. Furthermore normalizing the signal amplitude and especially performing the detection in angular domain makes it possible to reduce the dynamic range of the signal, reduce the number of signal branches from two to one, and take advantage over the periodic nature of angle information, thus making the computation resilient to overflows and reducing the number of bits required in computation.

It is demonstrated that the implementation complexity and power dissipation of the spatial sign cyclic correlator with angular domain computation is comparable with the energy detector, whereas the degradation in the performance is acceptable when compared to more complex detector structures. Therefore the high efficiency of the implementation makes it a excellent candidate for signal detector in mobile cognitive radio devices. However, the overall efficiency of the spectrum sensor is also strongly dependent on implementation of the RF front-end and the use cases, and therefore it is difficult to make unambiguous decision of the best implementation.

From the algorithm design point of view it has been demonstrated that it is not the absolute sensitivity in terms of ROC that defines the quality of the detector. Instead, the quality is a trade off between the sensitivity and implementation feasibility. It would be beneficial to take the possibilities for trade-offs into account already in the early phase of the algorithm design.

References

[1] S. Haykin, "Cognitive radio: Brain-empowered wireless communications," *IEEE J. Sel. Areas Commun.*, vol. 23, no. 2, pp. 201–220, Feb. 2005.

[2] I. Akyildiz, W.-Y. Lee, M. C. Vuran, and S. Mohanty, "Next generation/dynamic spectrum access/cognitive radio wireless networks: A survey," *Comput. Netw.*, vol. 50, no. 13, pp. 2127–2159, Sep. 2006.

[3] T. Yucek and H. Arslan, "A survey of spectrum sensing algorithms for cognitive radio applications," *IEEE Commun. Surv. Tutorials*, vol. 11, no. 1, pp. 116–130, 2009.

[4] P. Pawelczak, K. Nolan, L. Doyle, S. Oh, and D. Cabric, "Cognitive radio: Ten years of experimentation and development," *IEEE Commun. Mag.*, vol. 49, no. 3, pp. 90–100, Mar. 2011.

[5] A. Tkachenko, A. Cabric, and R. Brodersen, "Cyclostationary feature detector experiments using reconfigurable BEE2," in *IEEE Int. Symp. New Frontiers Dynam. Spectrum Access Netw.*, Apr. 2007, pp. 216–219.

[6] E. Axell, G. Leus, E. Larsson, and H. Poor, "Spectrum sensing for cognitive radio: State-of-the-art and recent advances," *IEEE Signal Process. Mag.*, vol. 29, no. 3, pp. 101–116, May 2012.

[7] R. Tandra and A. Sahai, "SNR walls for signal detection," *IEEE J. Sel. Topics Signal Process.*, vol. 2, no. 1, pp. 4–17, Feb. 2008.

[8] V. Turunen, M. Kosunen, M. Vaarakangas, and J. Ryynanen, "Correlation-based detection of OFDM signals in the angular domain," *IEEE Trans. Veh. Technol.*, vol. 61, no. 3, pp. 951–958, Mar. 2012.

[9] R. Tandra and A. Sahai, "Noise calibration, delay coherence and SNR walls for signal detection," in *Proc. 3rd IEEE Symp. New Frontiers Dynam. Spectrum Access Netw.*, Oct. 2008, pp. 1–11.

[10] D. Tse and P. Viswanath, *Fundamentals of Wireless Communication*. Cambridge, U.K.: Cambridge Univ. Press, 2005.

[11] S. Chaudhari, V. Koivunen, and H. V. Poor, "Autocorrelation-based decentralized sequential detection of OFDM signals in cognitive radios," *IEEE Trans. Signal Process.*, vol. 57, no. 7, pp. 2690–2700, Jul. 2009.

[12] A. V. Dandawatě and G. B. Giannakis, "Statistical tests for presence of cyclostationarity," *IEEE Trans. Signal Process.*, vol. 42, no. 9, pp. 2355–2369, Sep. 1994.

[13] K. Kokkinen, V. Turunen, M. Kosunen, S. Chaudhari, V. Koivunen, and J. Ryynänen, "On the implementation of autocorrelation-based feature detector," in *Proc. Int. Symp. Commun., Control Signal Process.*, 2010, pp. 1–4.

[14] E. Hogenauer, "An economical class of digital filters for decimation and interpolation," *IEEE Trans. Acoust., Speech, Signal Process.*, vol. 29, no. 2, pp. 155–162, Apr. 1981.

[15] H. Samueli, "An improved search algorithm for the design of multiplierless fir filters with powers-of-two coefficients," *IEEE Trans. Circuits Syst.*, vol. 36, no. 7, pp. 1044–1047, Jul. 1989.

[16] S. He and M. Torkelson, "A new approach to pipeline FFT processor," in *Proc. 10th Int. Parallel Process. Symp.*, Apr. 1996, pp. 766–770.

[17] J. Lindeberg, O. Väänänen, J. Pirkkalaniemi, M. Kosunen, and K. Halonen, "OFDM modulator with digital IF and on-chip D/A-converter," in *Proc. Custom Integrated Circuits Conf.*, Sep. 10–13, 2006, pp. 527–530.
[18] V. Turunen, M. Kosunen, A. Huttunen, S. Kallioinen, P. Ikonen, A. Pärssinen, and J. Ryynänen, "Implementation of cyclostationary feature detector for cognitive radios," in *Proc. Int. Conf. Cognitive Radio Oriented Wireless Netw. Commun.*, 2009, pp. 1–4.
[19] J. E. Volder, "The CORDIC trigonometric computing technique," *IRE Trans. Electron. Comput.*, pp. 330–334, Sep. 1959.
[20] C. Mazenc, X. Merrheim, and J.-M. Muller, "Computing functions cos^{-1} and sin^{-1} using CORDIC," *IEEE Trans. Comput.*, vol. 42, no. 1, pp. 118–122, Jan. 1993.
[21] E. Laulainen, L. Koskinen, M. Kosunen, and K. Halonen, "Compass tilt compensation algorithm using CORDIC," in *Proc. IEEE Int. Symp. Circuits Syst.*, 2008, May 2008, pp. 1188–1191.
[22] M. Kosunen, J. Vankka, M. Waltari, and K. Halonen, "A multicarrier QAM-modulator for WCDMA base-station with on-chip D/A converter," *IEEE Trans. Very Large Scale (VLSI) Syst.*, vol. 13, no. 2, pp. 181–190, Feb. 2005.
[23] J. Lundén, S. A. Kassam, and V. Koivunen, "Robust nonparametric cyclic correlation-based spectrum sensing for cognitive radio," *IEEE Trans. Signal Process.*, vol. 58, no. 1, pp. 38–52, Jan. 2010.
[24] S. Kallioinen, M. Vääräkangas, P. Hui, J. Ollikainen, I. Teikari, A. Pärssinen, V. Turunen, M. Kosunen, and J. Ryynänen, "Multi-mode, multi-band spectrum sensor for cognitive radios embedded to a mobile phone," in *Proc. 6th Int. ICST Conf. Cognitive Radio Orient. Wireless Netw. Commun.*, 2011, Jun. 2011, pp. 236–240.
[25] I. Kuon and J. Rose, "Measuring the gap between FPGAs and ASICs," *Proc. IEEE Trans. Comput.-Aided Design Integr. Circuits Syst.*, vol. 26, no. 2, pp. 203–215, Feb. 2007.

Marko Kosunen (S'97–M'07) received the M.Sc., L.Sc., and D.Sc. (with honors) degrees from Helsinki University of Technology, Espoo, Finland, in 1998, 2001, and 2006, respectively.

He is currently a Senior Researcher at the Department of Micro and Nanosciences, Aalto University, Espoo, Finland. His expertise is in implementation of the wireless transceiver DSP algorithms and communication circuits. He is currently working on implementations of cognitive radio spectrum sensors, digital intensive transceiver circuits, and medical sensor electronics.

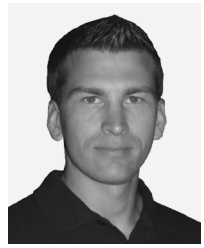

Vesa Turunen (S'11) received the M.Sc. (Tech) degree in microelectronic circuit design from the Department of Electrical and Communications Engineering, Helsinki University of Technology, Espoo, Finland, in 2007. He is currently pursuing a D.Sc.(Tech) degree at the School of Electrical Engineering, Aalto University, Espoo, Finland.

In 2012, he joined Renesas Mobile, Helsinki, Finland, where he currently works with the state-of-the-art mobile transmitters.

Kari Kokkinen received the M.S. degree from the Department of Micro- and Nanosciences, School of Electrical Engineering, Aalto University, Espoo, Finland, in 2010.

He joined the Renesas Mobile Oulu, Oulu, Finland, in January 2012, where he is currently working as a Design Engineer. His research interests include LTE, cognitive radio and mobile radar applications.

Jussi Ryynänen (S'99–M'04) was born in Ilmajoki, Finland, in 1973. He received the M.S., Licentiate of Science, and Doctor of Science degrees in electrical engineering from Helsinki University of Technology, Helsinki, Finland, in 1998, 2001, and 2004, respectively.

He is currently working as an Associate Professor at the Department of Micro- and Nanosciences, School of Electrical Engineering, Aalto University, Espoo, Finland. His main research interests are integrated transceiver circuits for wireless applications. He has authored or coauthored over 90 refereed journal and conference papers in the areas of analog and RF circuit design. He holds six patents on RF circuits.